

CONCEPTUAL PERFORMANCE AND MASS ASSESSMENT OF AN OPEN FAN ENGINE FOR THE DLR-F25 AIRCRAFT

Patrick Wehrel[1], Jannik Häßy[1], Rainer Schnell[1] & Sebastian Wöhler[2]

[1]German Aerospace Center (DLR), Institute of Propulsion Technology, Cologne 51147 Germany
[2]German Aerospace Center (DLR), Institute of System Architectures in Aeronautics, Hamburg, 21129, Germany

Abstract

Open propulsion systems are promising concepts for future aircraft due to their high propulsive efficiency. Currently, intensive research is being conducted on a civil open fan configuration with adjustable rotor and stator blades, which are mounted at the front of the envisaged propulsion system upstream of the core engine inlet. This paper assesses the performance and mass of such an open fan engine for a short-medium range aircraft in the early phase of conceptual design. The performance of the core engine is modeled by a multidisciplinary design process and CFD-generated maps are used to describe the operating behavior of the propulsor. In detail, there are separate maps for the installed propulsor efficiency, the rotor total pressure ratio and the rotor total temperature ratio. As part of this work, an open fan performance model and a 2D core engine geometry model are created. The geometry model generation is based on a sketching process, which applies thermodynamic cycle data as well as a parametrized reference engine geometry. To estimate the core engine, gearbox and propulsor masses, a correlation-based methodology is utilized. Several core engine technology limitations and a suitable design scheme are introduced in order to determine an open fan design with minimum thrust-specific fuel consumption. Moreover, a variation of the design propulsor rotational speed and power coefficient is conducted. After the open fan design determination, the corresponding preliminary propulsor, performance and mass results are evaluated in detail. This includes a sensitivity analysis of the performance and mass results to aircraft installation effects. As a final step, future propulsor design goals are defined.

Keywords: Conceptual Design, CFD, Mass, Open Fan, Performance

1. Introduction

In view of the climate goals and strategies, such as those published in the European reports *Flight Path 2050* [1] or *Fly the Green Deal* [2], reducing fuel consumption and long-term decarbonization of aircraft are crucial for achieving these objectives. Over the past decades, conventional turbofan engines have been continuously optimized, but the efficiency gains enabled by incremental improvements are gradually beginning to level off. Therefore, there is a strong need for alternative, revolutionary propulsion concepts in order to meet the envisaged climate targets.
Open propulsion concepts are a promising approach for future aircraft and are currently being primarily investigated for civil aviation applications [3, 4]. In contrast to conventional turbofan engines, these concepts eliminate the nacelle surrounding the fan/propulsor, leading to a significant increase in bypass ratio and thus propulsive efficiency. However, this unducted design is also accompanied by its own challenges, like higher noise levels or issues caused by the wing integration. Open propulsion concepts can be generally divided into puller and pusher configurations. In the first arrangement, the propulsor is installed in front of the core engine and pulls the aircraft forward, whereas in the second approach, the propulsor is mounted behind the core engine and pushes the aircraft.

Initial prototypes of open propulsion concepts were already developed and tested in the 1980s as a response to high fuel prices. Well-known examples are the *GE36 Unducted Fan* [5] and the *Pratt &*

Whitney/Allison 578-DX [6], both counter-rotating pusher configurations featuring two rows of coaxial blade rows rotating in opposite directions. A main driver for the counter-rotating architecture is the recovery of the swirl generated by the first rotor. Due to falling oil prices and high noise emissions, the development of these prototypes was discontinued at the end of the 1980s.
In the 2010s, research into the counter-rotating pusher concept was once again intensified, bundled under the acronym CROR (counter-rotating open rotor). A key objective of numerous CROR activities was the reduction of noise levels. Important contributions were achieved in the *Continuous Lower Energy, Emissions and Noise (CLEEN)* program initiated by the Federal Aviation Administration (FAA) [7] as well as in the *NASA Environmentally Responsible Aviation (ERA)* project [8], with a corresponding performance and mass assessment of a CROR engine published in [9]. Furthermore, the DLR conducted an aerodynamic and acoustic optimization of a CROR propulsor within the European *valiDation of Radical Engine Architecture systeMs (DREAM)* project [10]. In 2017, a major milestone was achieved when Safran ground tested a CROR demonstrator [11]. As a result of the CROR initiatives, noise emissions have been significantly reduced compared to those of the prototypes developed in the 1980s. However, the investigated CROR engine design was relatively heavy, in particular the propulsor assembly [9].
Building upon prior efforts and findings, current research on open propulsion systems focuses primarily on a puller configuration, which has been established as the open fan within the *CFM RISE (Revolutionary Innovation for Sustainable Engines)* program [12]. The open fan concept features a single rotor followed by a non-rotating stator [11, 13]. Both the rotor and stator blades are equipped with variable pitch control and are installed at the front of the envisaged propulsion system. Analogous to the second rotor of the counter-rotating architecture, the stator is used for swirl recovery. A first performance and mass estimation of an open fan engine for a single-aisle, narrow-body aircraft was conducted as part of the *NASA Hybrid Thermally Efficient Core (HyTEC)* project [14].

This paper also contributes to the investigation of open fan engines and presents the current state of a conceptual performance and mass assessment conducted by DLR. Figure 1 illustrates the DLR open fan engine, which is designed in the context of a short-medium range aircraft. The aircraft is also presented in Figure 1 and was originally established as the DLR-F25 research baseline, but in conjunction with a next-generation turbofan engine [15]. Section 2 introduces the methodology applied for the performance and mass assessment of the DLR open fan engine. The corresponding preliminary results are presented in Section 2.6.

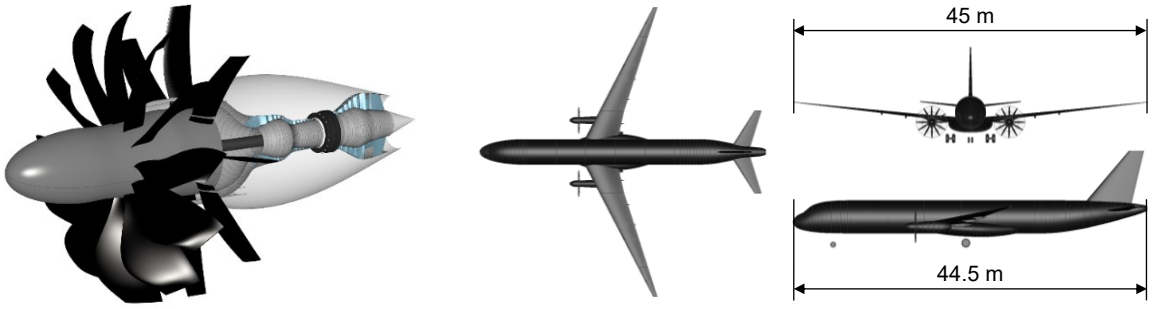


Figure 1 – DLR open fan engine (left) and three view of the DLR-F25 open fan configuration (right, stator blades and pylon are not visualized).

2. Methodology

This section describes the methodology used to assess the performance and mass of the DLR open fan engine presented in Figure 1. All conceptual engine design tools in terms of performance modeling (see Section 2.3) as well as geometry and mass estimation (see Section 2.4) are integrated in the DLR framework GTlab (Gas Turbine Laboratory), which is developed for multidisciplinary, collaborative research in the field of aircraft propulsion [16, 17]. Moreover, CFD-based propulsor maps are generated by means of the DLR CFD framework TRACE [18] and are subsequently processed in

order to apply them on overall engine level (see Section 2.5 and 2.6).

2.1 Open Fan Engine Requirements

The engine requirements for the DLR-F25 open fan configuration regarding thrust, shaft power offtake and bleed air are provided by the overall aircraft design using the process described in [15] and are presented in Table 1 for different operating points. These requirements constitute the basis for the conceptual engine design process introduced in the following sections. In detail, the operating points maximum takeoff (MTO), end of field (EOF), second segment (2ndSeg), top of climb (TOC) and mid-cruise (Mid-CR) are considered. MTO, EOF, 2ndSeg and TOC originate from the aircraft design mission, whereas Mid-CR is part of the evaluation mission. The Mach number of 0.78 at Mid-CR is equal to that of the DLR-F25 turbofan configuration [15].

Table 1 – Engine requirements for the DLR-F25 open fan configuration.

Parameter	Unit	MTO	EOF	2ndSeg	TOC	Mid-CR
Aircraft Mission	[-]	Design	Design	Design	Design	Evaluation
Flight Level	[100ft]	0	0	4	350	370
Altitude	[m]	0	11	122	10668	11277.6
Mach-Number	[-]	0.0	0.226	0.224	0.76	0.78
Delta Temp. ISA	[K]	15	15	15	10	0
Engine Rating	[-]	MTO	MTO	MTO	MCL	MCR
Thrust	[kN]	134.1	74.6	82.1	22.0	17.1
Thrust	[klbf]	30.1	16.8	18.5	4.9	3.8
Shaft Power Offtake	[kW]	-95	-95	-95	-50	-50
Bleed Air Offtake	[kg/s]	0.0	0.0	0.0	0.425	0.425

2.2 Open Fan Engine Bookkeeping

The correct bookkeeping of the occurring forces on the open fan engine is crucial in order to create a valid engine design for the thrust requirements shown in Table 1. Since the net thrust formulation of an open fan engine is slightly different from that of a conventional turbofan due to the open fan rotor in front of the core engine inlet, the individual gross thrusts F_G and drags F_D are specified below and are then combined into the net thrust F_N. All relevant forces are also visualized schematically in Figure 2.

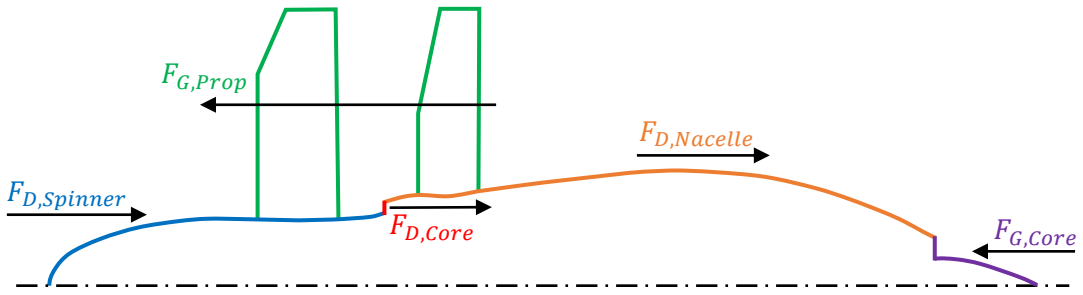


Figure 2 – Schematic illustration of the open fan engine bookkeeping.

As shown in Eq. (1), the net thrust of the propulsor $F_{N,Prop}$ is defined here as the difference between propulsor gross thrust $F_{G,Prop}$ generated by the blading and the drag of the spinner and nacelle $F_{D,Spinner} + F_{D,Nacelle}$. The propulsor net thrust $F_{N,Prop}$ is also used in the calculation of the installed propulsor efficiency $\eta_{Prop,Inst}$ introduced as part of the propulsor maps (see Eq. (10) and Figure 9). Accordingly, the uninstalled efficiency is based on the propulsor gross thrust $F_{G,Prop}$ and is referred to as blade-only efficiency in an accompanying paper [19]. The ratio between the installed uninstalled propulsor efficiency is specified as installation efficiency. Details on these efficiencies and the influence of the nacelle drag on them are presented in [19]. In this paper, only the installed propulsor efficiency $\eta_{Prop,Inst}$ is applied, which is an input for the performance model of the open fan engine (see Figure 3) and is provided by [19] in the form of a CFD-generated open fan propulsor map (see Figure 9).

$$F_{N,Prop} = F_{G,Prop} - \left(F_{D,Spinner} + F_{D,Nacelle}\right) \tag{1}$$

Following the same approach as in Eq. (1), the core engine net thrust $F_{N,Core}$ is equal to the core engine gross thrust $F_{G,Core}$ subtracted by the core engine drag $F_{D,Core}$ (see Eq. (2)). In contrast to turbofan engines, where the pressure force term $A_{Core,In}\left(p_{Core,In} - p_{Air}\right)$ is normally not considered within the core engine drag $F_{D,Core}$, this is crucial for the open fan engine, since the core inlet pressure $p_{Core,In}$ does not correspond to the freestream pressure p_{Air} due to the open fan rotor (see total pressure ratio map in Figure 9). The core inlet area $A_{Core,In}$ is provided by the CFD model see (Section 2.4 and Table 4). The reaction force term $\dot{m}_{Core,In}c_{Core,In}$ also exists in the net thrust definition of turbofan engines and corresponds to the time derivative of the inlet momentum.

$$F_{N,Core} = F_{G,Core} - F_{D,Core} = F_{G,Core} - \dot{m}_{Core,In}c_{Core,In} - A_{Core,In}\left(p_{Core,In} - p_{Air}\right) \tag{2}$$

The gross thrust of the core engine nozzle $F_{G,Core}$ is determined in the same way as for turbofan engines (see Eq. (3)). In performance models (see Figure 3), a discharge and velocity coefficient are usually applied in order to approximate the flow state regarding c_8 and A_8 of a real nozzle configuration with a plug and flow-guiding elements [20, 21].

$$F_{G,Core} = \dot{m}_8 c_8 + A_8(p_8 - p_{Air}) \tag{3}$$

Finally, the net thrust of the open fan engine F_N is calculated by adding the propulsor net thrust $F_{N,Prop}$ and the core engine net thrust $F_{N,Core}$:

$$F_N = F_{N,Prop} + F_{N,Core} \tag{4}$$

2.3 Performance Modeling

In order to calculate thermodynamic cycle data for the open fan engine, a performance model is created by means of the GTlab performance module. The performance model is illustrated in Figure 3 and consists of a conventional two-shaft core engine marked in green and a propeller that is used to approximate the open fan propulsor in this early design stage.

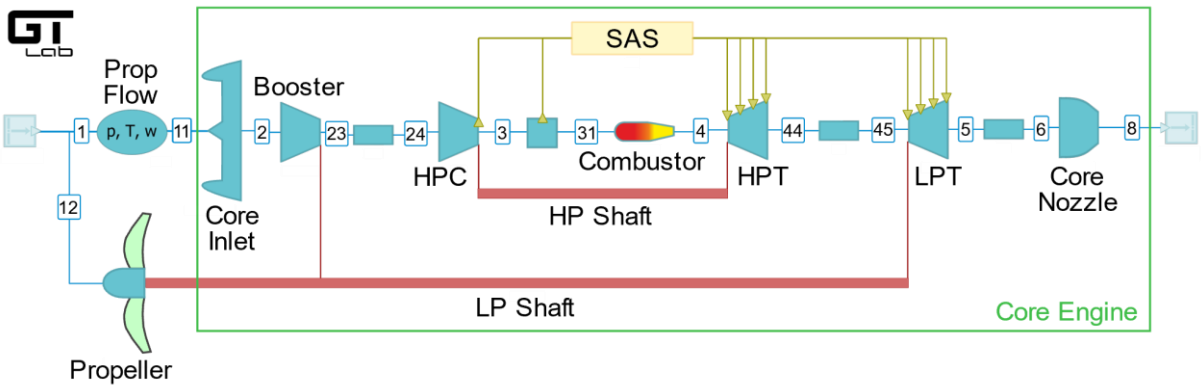


Figure 3 – Performance model of the open fan engine.

The propeller module is supplied with aerodynamic design data in terms of rotational speed, advance ratio and power coefficient as well as propulsor maps. Both the aerodynamic design data and the maps are provided by a CFD model (see Section 2.4 and Section 3.1). In detail, three maps are used to describe the operating behavior of the propulsor. The integration of an installed efficiency map enables the calculation of the propulsor net thrust $F_{N,Prop}$ (see Eq. (1)) for different flight conditions. Moreover, two maps are applied that describe the change in total pressure and temperature between the core engine inlet and the freestream condition before the open fan rotor (see station 1 and 11 in Figure 3). These maps are linked to a flow modifier before the core engine inlet (see prop flow element in Figure 3), which transfers the respective total pressure and temperature ratios to the core engine flow in order to predict correct flow states in the core engine inlet. The propeller is connected to the core engine through a gearbox and the low-pressure shaft. Note that the gearbox is integrated into the propeller and is thus not visible in the performance model (see Figure 3).

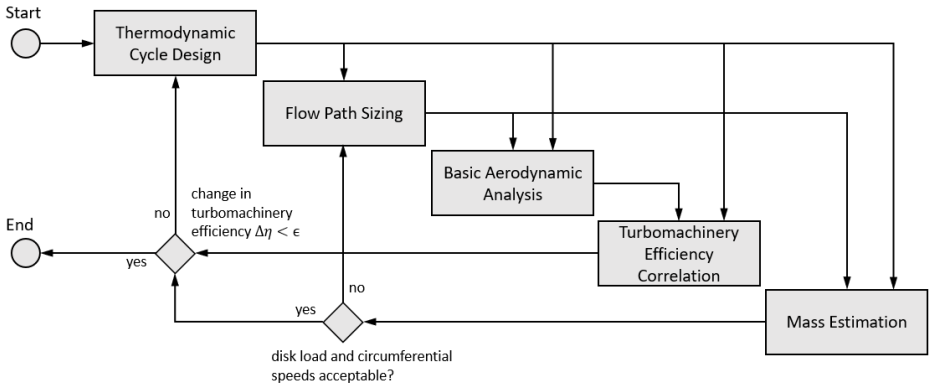


Figure 4 – Multidisciplinary engine design process [15].

For the core engine, a multidisciplinary design process is applied that is presented in Figure 4. Based on thermodynamic cycle data, a preliminary flow path sizing procedure is conducted, which is detailed in Section 2.4. Subsequently, basic aerodynamic parameters are calculated for each turbomachinery, such as flow coefficient or stage loading. These are then used together with the performance data to predict the turbomachinery efficiencies by means of several correlations. The aerodynamic analysis and the efficiency correlations are described in [22]. Finally, the masses of the core engine components are estimated by using a methodology that is also introduced in Section 2.4. The core engine design is converged when all circumferential speeds and disk loads are below their respective limit (see Section 3.1.1) and when the turbomachinery efficiency changes are below a user-defined convergence threshold. Otherwise, modifications in the performance model or in the flow path sizing procedure are necessary to fulfill these requirements.

2.4 Geometry Modeling and Mass Estimation

In this paper, only the geometry of the core engine of the open fan propulsion system is modeled in detail for now (see Figure 3). Therefore, a sketching process is applied that is able to generate 2D geometry models (see Figure 10), which also serves as the basis for a subsequent mass estimation of the core engine components. The process is illustrated in Figure 5 and uses thermodynamic cycle data as well as parametrized characteristics of a reference engine geometry, such as blade aspect or taper ratio. Hence, each modification in the performance model (see Figure 3) is reflected in the 2D geometry model. Details on this sketching process are provided in [23, 24]. The same reference core engine geometry as in [15] is selected in this paper, which represents the knowledge of a state-of-the-art geared turbofan for short-medium range aircraft.

By using the 2D geometry model, thermodynamic cycle data and the GTlab material database, the mass of each core engine component is estimated (see Figure 5). The mass estimation tool applied in this paper originates from a correlation-based methodology published by *Klees and Fishbach* [25] and was enhanced by *Häßy and Schmeink* [23]. Details on the mass estimation process are also provided in [23].

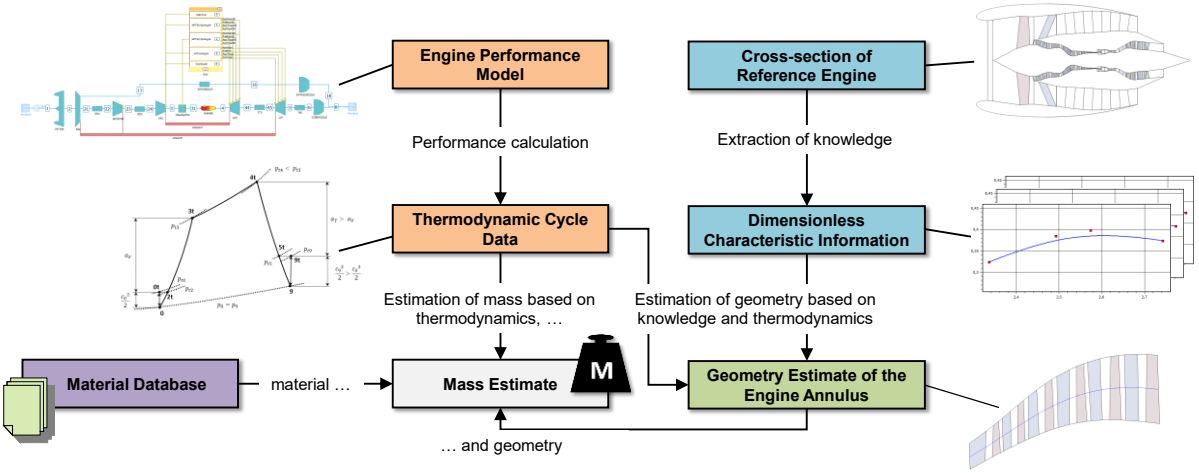


Figure 5 – Geometry modeling and mass estimation process [23].

The gearbox mass $m_{Gearbox}$ in [lb] is calculated by means of a correlation from *Hendricks and Tong* [9], which was originally used in [9] for a CROR engine and considers the maximum propulsor shaft power P in [shp], the maximum propulsor rotational speed n_{Prop} in [rpm] and the corresponding gear ratio $i = n_{Prop}/n_{Core}$:

$$m_{Gearbox} = -37.4262 + 116.3297 \cdot \left[\left(\frac{P}{n_{Prop}}\right)^{0.75} \cdot \left(\frac{1}{i}\right)^{0.15}\right] \tag{5}$$

To the authors' knowledge, there are currently no correlations in the public literature that are tailored for the mass estimation of the open fan propulsor, since this a novel and emerging engine architecture. Nevertheless, the propulsor mass is crucial, as it accounts for a significant proportion of the total engine weight (see Table 6). Therefore, a mass estimation correlation for conventional propellers is used in order to generate preliminary results as long as no more suitable correlations are available. According to *Strack et al*. [12], the mass of the propulsor rotor assembly $m_{Prop,Rot}$ in [lb] is estimated based on the rotor diameter D_{Rot} in [ft], the number of rotor blades B_{Rot}, the total rotor activity factor $AF_{Tot,Rot} = AF_{Rot} \cdot B_{Rot}$, the maximum circumferential rotor tip speed $u_{Tip,Rot}$ in [ft/sec], the maximum propulsor shaft power P in [shp] and the rotor sweep angle $sweep_{Rot}$ in [°] (see Eq. (6)). In addition, an overall technology factor TF is included in Eq. (6), representing the technological advancements since the correlation's publication in 1982. A technology factor of 0.833 is determined in studies on a DLR-internal state-of-the-art turboprop engine, which is also applied here. Note that the correlation accounts for the mass of the entire propulsor rotor assembly $m_{Prop,Rot}$,

including variable pitch control and other sub-components.

$$m_{Prop,Rot} = \left[3.37 \cdot 10^{-4} \cdot D_{Rot}^{1.846} \cdot B_{Rot}^{-0.05} \cdot AF_{Tot,Rot}^{0.75} \cdot u_{Tip,Rot}^{0.3} \cdot P^{0.327} \cdot \left[1 + \left(\frac{sweep_{Rot}}{40}\right)\right]\right] \cdot TF \quad (6)$$

The mass of the propulsor stator assembly $m_{Prop,Stat}$ is estimated utilizing the same approach as in Eq. (6) for simplicity, but with the stator design parameters in terms of diameter, blade number, total activity factor and sweep angle as well as an empirical weight factor that is set to 0.6 (see Eq. (7)). The rotor parameters regarding $u_{Tip,Rot}$ and P remain unchanged in Eq. (7). Analogous to Eq. (6), the correlation considers the mass of the entire propulsor stator assembly $m_{Prop,Stat}$ with the variable pitch control and all sub-components.

$$m_{Prop,Stat} = 0.6 \cdot m_{Prop,Rot}\left(D_{Stat},\ B_{Stat},\ AF_{Tot,Stat},\ sweep_{Stat}\right) \quad (7)$$

2.5 Propulsor Map Generation

The availability of propulsor maps for the propeller module of the performance model (see Figure 3) is essential in order to generate reliable performance results. Hence, these maps are calculated by a CFD model of the open fan engine, which is illustrated in Figure 6. The model was created as part of the CFD investigations conducted by *Schnell et al.* published in an accompanying paper [19]. One objective of [19] is to discuss two design strategies for the open fan propulsor and to analyze the influence of the nacelle drag on these strategies. The first propulsor configuration is optimized for the maximization of the uninstalled efficiency and thus the propulsor gross thrust $F_{G,Prop}$ generated solely by the blading (see Figure 2). In contrast, the other configuration is designed for the minimization of the nacelle drag $F_{D,Nacelle}$ (see Figure 2). Since a maximum installed propulsor efficiency (see Eq. (10)) and consequently a maximum propulsor net thrust $F_{N,Prop}$ (see Eq. (1)) are crucial for the overall engine performance, a further combined design is created in [19] that includes the blade geometries of the “maximum blade-only efficiency variant” and the nacelle geometry of the “minimum drag variant”. The combined design is also applied in this paper in order to generate the required propulsor maps.

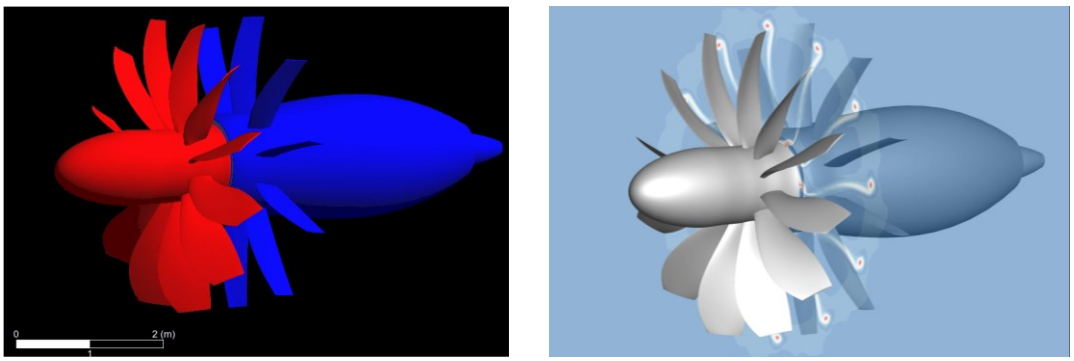


Figure 6 – DLR CFD model of the open fan engine (left) and contour of entropy in an axial plane upstream the core engine inlet (right) [19].

As mentioned in Section 2.3, three maps are integrated in the propeller module of the performance model (see Figure 3). In detail, there are separate maps for the installed propulsor efficiency $\eta_{Prop,Inst}$, the rotor total pressure ratio $p_{t,11}/p_{t,1}$ and the rotor total temperature ratio $T_{t,11}/T_{t,1}$ (see Figure 9). Each map is arranged in such a way that the advance ratio J is shown on the x-axis and the power coefficient c_p on the y-axis, while the respective parameter of interest is displayed as a carpet plot. The introduced quantities are defined as follows:

$$J = \frac{V_{Air}}{n_{Prop} D_{Rot}} \tag{8}$$

$$c_p = \frac{P}{\rho_{Air} n_{Prop}^3 D_{Rot}^5} \tag{9}$$

$$\eta_{Prop,Inst} = \frac{F_{N,Prop} V_{Air}}{P} \tag{10}$$

$$\frac{p_{t,11}}{p_{t,1}} = \frac{p_{t,Core,In}}{p_{t,Air}} \tag{11}$$

$$\frac{T_{t,11}}{T_{t,1}} = \frac{T_{t,Core,In}}{T_{t,Air}} \tag{12}$$

Note that the freestream fluid velocity V_{Air} corresponds to the flight speed. The remaining freestream parameters are calculated accordingly. All other quantities are already introduced in Section 2.2 and Section 2.4. In the performance model (see Figure 3), the freestream conditions are stored in station 1 and station 12, respectively. Station 11 represents the core engine inlet flow state.

The propulsor maps used in this paper are calculated by means of a methodology described in an accompanying paper [19]. In summary, a map is generated by varying the advance ratio J for different rotor and stator pitch settings (see Eq. (8)). Therefore, the rotational speed n_{Prop} is modified and the flight speed is kept constant for a fixed pitch configuration. Since propulsor maps are not inherently Mach similar, it is important to ensure that the advance ratio J and the corresponding map data of different pitch lines are computed at the correct flight Mach number and respective velocity V_{Air} [19]. All pitch lines are created under sea-level standard conditions. To reduce the number of dimensions of the propulsor maps and thereby facilitate the modeling of the overall engine performance, only the rotor pitch is provided in the map (see Figure 9). The stator pitch is modified indirectly by using an adjustment logic described in [19]. Consequently, the propulsor maps applied here inherently contain a stator pitch change that is matched to the respective rotor pitch. Further details on the map generation as well as other approaches for an advance ratio variation are presented in [19].

2.6 Propulsor Map Processing

After the CFD-based generation of the propulsor maps, these have to be processed in order to apply them on overall engine level. This currently includes a map extrapolation toward low power coefficients (see Section 2.6.1) as well as a Reynolds number correction of the installed propulsor efficiency predictions (see Section 2.6.2).

2.6.1 Map Extrapolation

All propulsor maps are extrapolated in the direction of low power coefficients to be capable of calculating partial load operating points, such as flight idle (see Figure 9). Therefore, a three-step method is used, which is demonstrated in Figure 7. Note that the installed propulsor efficiency map shown in Figure 9 is used as an example for this purpose. First, the CFD-generated map data is read and converted into the required map format. The upper and lower map border are then smoothed using interpolated polynomials, whose degree is specified by the user. Finally, the propulsor map is linearly extrapolated between the smoothed lower border and an arbitrary minimum power coefficient $c_{p,min}$. For all maps, a value of $c_{p,min}$ = 0.0 is selected with the following values regarding the installed propulsor efficiency, the rotor total pressure ratio and the rotor total temperature ratio: $\eta_{Prop,Inst}$ = 0.0, $p_{t,11}/p_{t,1}$ = 1.0 and $T_{t,11}/T_{t,1}$ = 1.0. The slope of the linear extrapolation is determined at the lower border and is kept constant throughout the extrapolation area. This approach appears similar to the one used in [13].

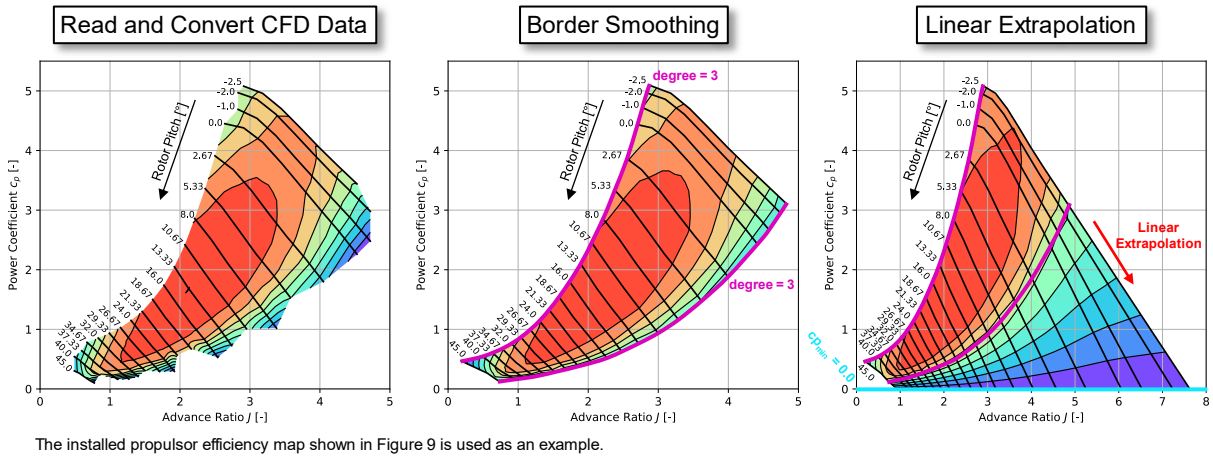


Figure 7 – Three-step propulsor map extrapolation method consisting of CFD data reading and conversion (left), border smoothing (center), and linear extrapolation (right).

2.6.2 Reynolds Number Correction

Due to Reynolds effects, the prediction of the propulsor efficiency map has to be corrected when the map is used in combination with operating points at high flight levels or Mach numbers, since all propulsor maps are calculated under sea-level standard (SLS) conditions (see Section 2.4). Therefore, a method that is based on the Reynolds number index is applied. Details on this approach are provided in [20]. The Reynolds number correction method is calibrated by determining the efficiency difference between the CFD results under cruise conditions and the map efficiency for the same advance ratio and power coefficient. Typically, the efficiency prediction of the SLS map is better than the actual cruise efficiency, which is caused by Reynolds effects. The Reynolds number correction method computes an efficiency delta as a function of the Reynolds number index, which is calibrated by ensuring that the SLS map efficiency matches the actual cruise efficiency. Since the Reynolds number index only depends on the flight conditions, it is possible to calculate a Reynolds efficiency delta for any operating point by means of the calibrated model, which is also conducted in this paper.

3. Preliminary Results

This section presents the current state of the conceptual performance and mass assessment of the DLR open fan engine. The preliminary results are generated with the methodology introduced in Section 2. First, the design determination of the open fan engine is described (see Section 3.1). The propulsor results are then summarized (see Section 3.2), followed by the performance and mass results (see Section 3.2). Moreover, the sensitivity of aircraft installation effects to the performance and mass results is analyzed (see Section 3.4). Finally, future propulsor design goals and their impact on the overall open fan design are considered (see Section 3.5).

3.1 Open Fan Design Determination

The focus of this section is the open fan design determination. Initially, the core engine technology limitations used within the multidisciplinary engine design process (see Figure 4) are introduced (see Section 3.1.1). Subsequently, the applied open fan design scheme is described (see Section 3.1.2), which reveals the importance of a propulsor rotational speed and power coefficient variation. Hence, such a study is conducted in conclusion (see Section 3.1.3).

3.1.1 Core Engine Technology Limitations

Table 2 summarizes the core engine technology limits that are considered within the multidisciplinary engine design process (see Figure 4). The limits originate from the DLR-F25 turbofan configuration [15] and represents an entry in service (EIS) of 2035. For each engine rating, there is

a threshold for the high-pressure turbine (HPT) rotor inlet temperature, also referred to as T41. For the high-pressure compressor (HPC), the HPC outlet temperature (T3) and the blade height at the HPC outlet are restricted, which both affect the determination of the overall pressure ratio of the core engine. Finally, there are different limits regarding the permissible circumferential speeds and disk loads of the HPC and low-pressure turbine (LPT). These are used to determine the maximum tolerable rotational speeds of the high-pressure (HP) and low-pressure (LP) shaft.

Table 2 – Core engine technology limits for EIS 2035 from the DLR-F25 turbofan configuration [15].

Component	Parameter	Rating	Unit	Limit
HPT	T41	MTO	[K]	2050
	T41	MCL	[K]	1725
	T41	MCR	[K]	1600
HPC	Max. T3	All	[K]	1000
	Min. Outlet Blade Height	-	[mm]	11.5
HP Shaft	Max. HPC Inlet Mean Circumferential Speed	All	[m/s]	420
	Max. HPT Disk Load	All	[MPa]	600
LP Shaft	Max. LPT Outlet Mean Circumferential Speed	All	[m/s]	370
	Max. LPT Disk Load	All	[MPa]	500

3.1.2 Open Fan Design Scheme

This section presents the scheme used to determine the open fan design, taking into account the core engine technology limits introduced in Table 2. The scheme is summarized in Table 3 and is applied in the context of the multidisciplinary engine design process illustrated in Figure 4. Among the operating points listed in Table 1, Mid-CR is selected as the engine design point. Hence, the remaining operating points are considered under off-design conditions. Note that it is currently not possible to calculate MTO, since the CFD-generated propulsor maps contain no data at an advance ratio of zero, where MTO is located (see Figure 9). In detail, the determination of the engine design point is based on the following approaches and conditions:

- The design pressure ratio of the booster $\Pi_{Booster}$ and the HPC Π_{HPC} are determined by setting the total HPC outlet temperature $T_{t,3}$ at Mid-CR to 796 K, by specifying the quotient between the booster and HPC pressure ratio $\Pi_{Stage,Booster}/\Pi_{Stage,HPC}$, and by considering the compressor stage numbers of the 2D open fan core engine geometry model (see Figure 10). The $T_{t,3}$-condition is adopted from the DLR-F25 turbofan configuration [15], where it leads to low nitrogen oxides (NOx) emissions. Consequently, this is an early assumption that simplifies the initial design selection and can be examined in greater detail later, once emission models have been integrated into the open fan design process. The overall pressure ratio (OPR) results predominantly from $\Pi_{Booster}$ and Π_{HPC}.
- By limiting the total HPT rotor inlet temperature $T_{t,41}$ at TOC according to the MCL limit of 1725 K (see Table 2), the fuel to air ratio FAR of the combustor and thus the $T_{t,41}$ are determined at the engine design point. Note that TOC is currently the hottest operating point (see Table 5).
- The core engine inlet mass flow $\dot{m}_1$ (see station 1 in Figure 3) is calculated based on the net thrust requirement of 17.1 kN at Mid-CR (see Table 1).

- For quantifying the design turbomachinery efficiencies of the core engine ($\eta_{Booster}$, η_{HPC}, η_{HPT} and η_{LPT}), the turbomachinery efficiencies correlations [22] introduced as part of Section 2.3 are used.
- The design rotational speed of the HP shaft n_{HPS} and the LP shaft n_{LPS} are determined by maximizing the rotational shaft speeds in compliance with the permissible circumferential speeds and disk loads of the HPC and LPT (see Section 2.3 and Table 2).
- Regarding the propulsor, the design rotational speed n_{Prop} and power coefficient c_p have to be specified in order to set the design point in the propulsor maps (see Figure 9). Consequently, it is possible to calculate all corresponding propulsor properties at the design point, such as the rotor pitch, the advance ratio J (see Eq. (8)), the propulsor shaft power P (see Eq. (9)), the installed propulsor efficiency $\eta_{Prop,Inst}$ (see Eq. (10)), the rotor total pressure ratio $p_{t,11}/p_{t,1}$ (see Eq. (11)) and the rotor total temperature ratio $T_{t,11}/T_{t,1}$ (see Eq. (12)). The propulsor net thrust $F_{N,Prop}$ results from Eq. (10) and the calculated propulsor shaft power P. Note that the rotor diameter D_{Rot} of 4 m is adopted from an accompanying paper [19] and is not modified within this paper. The only propulsor parameter varied in this paper are the design rotational speed n_{Prop} and power coefficient c_p in order to minimize the thrust-specific fuel consumption (TSFC) at Mid-CR. This parameter variation and the associated determination of the optimal n_{Prop} and c_p values are presented in the following section.

Table 3 – Summary of the DLR open fan design scheme.

Design Parameter @Mid-CR	Approach / Condition
$\Pi_{Booster}$, $\Pi_{HPC} \rightarrow OPR$	$T_{t,3}@Mid\text{-}CR = 769\ K$ $\frac{\Pi_{Stage,Booster}}{\Pi_{Stage,HPC}}$ Specification & Compressor Stage Numbers
$FAR \rightarrow T_{t,41}$	$T_{t,41}@TOC = 1725\ K$
$\dot{m}_1$	$F_N@Mid\text{-}CR = 17.1\ kN$
$\eta_{Booster}$, η_{HPC}, η_{HPT}, η_{LPT}	Turbomachinery Efficiencies Correlations [22] (see Section 2.3)
n_{HPS}, n_{LPS}	Maximum Circumferential Speeds and Disk Loads (see Section 2.3 and Table 2)
n_{Prop}, $c_p \rightarrow$ Propulsor Properties	$TSFC_{min}@Mid\text{-}CR$ in Propulsor n_{Prop}-c_p-Variation (see Section 3.1.3)

3.1.3 Propulsor Rotational Speed and Power Coefficient Variation

The variation of the design propulsor rotational speed n_{Prop} and power coefficient c_p is presented in Figure 8 based on the installed propulsor efficiency map from Figure 9. c_p influences the y-position of the design point in the map, while an increase in n_{Prop} moves the design point towards lower advance ratios (see Eq. (8)). Be advised that Mach similarity is currently not entirely maintained for low advance ratios, which is a challenging task within the propulsor map generation (see Section 2.5). Hence, it is expected that the propulsor efficiency might be compromised in this map region. As emphasized in Table 8, the target of the n_{Prop}-c_p-variation is the minimization of the TSFC at Mid-CR. Note that the installed TSFC is considered in this paper that includes the drag of the spinner $F_{D,Spinner}$ and the nacelle $F_{D,Nacelle}$ in the calculation of the net thrust F_N (see Eq. (1) and

Eq. (4)). Hence, the installed thrust-specific fuel consumption of an open fan engine $TSFC$ is defined here as follows:

$$TSFC = \frac{\dot{m}_{Fuel}}{F_N} = \frac{\dot{m}_{Fuel}}{F_{N,Prop}+F_{N,Core}} = \frac{\dot{m}_{Fuel}}{(F_{G,Prop}-F_{D,Spinner}-F_{D,Nacelle})+(F_{G,Core}-F_{D,Core})} \tag{13}$$

$\dot{m}_{Fuel}$ is the combustor fuel mass flow and the computation of the core engine gross thrust $F_{G,Core}$ and the core engine drag $F_{D,Core}$ for an open fan engine is provided in Eq. (2).

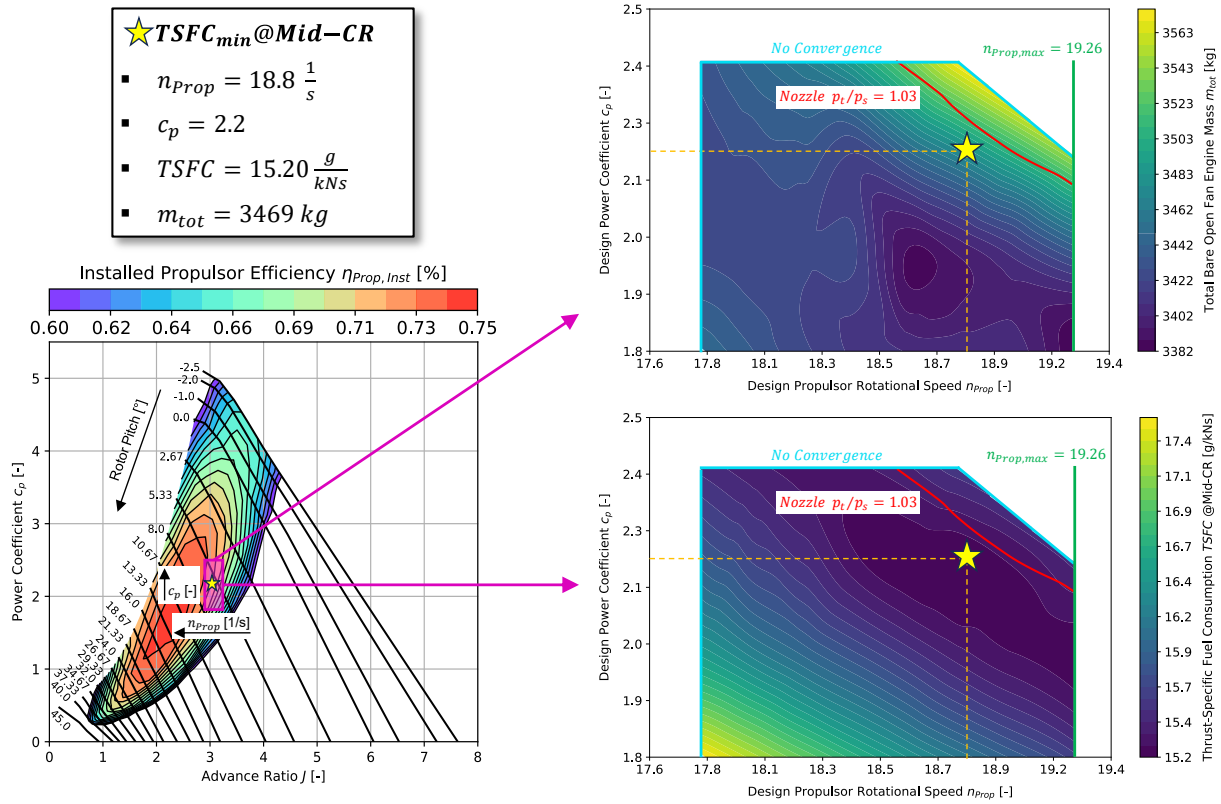


Figure 8 – Variation of the design propulsor rotational speed and power coefficient to minimize the thrust-specific fuel consumption at Mid-CR.

The contour plots of the TSFC and the total bare open fan engine mass generated in the n_{Prop}-c_p-variation are shown on the right side of Figure 8. Additional contour plots of other important performance and mass parameters are provided in the Appendix (see Figure 12). Although the range of the n_{Prop}-c_p-variation within the propulsor maps is small (see left side of Figure 8), the impact on the TSFC is significant with changes of more than 10%, which highlights the relevance of this variation. As indicated by the contour plot of the ratio between the core engine net thrust and the open fan net thrust $F_{N,Core}/F_N$ (see Figure 12), both n_{Prop} and c_p can be used to determine how much net thrust is generated by the propulsor and how much by the core engine. If the core engine produces insufficient thrust, the nozzle pressure ratio p_t/p_s becomes very low at flight idle (see Figure 12). The flight idle operation point is introduced in Section 3.2 and is defined at the advance ratio of Mid-CR and a power coefficient of zero (see Figure 9). Therefore, this work assumes that p_t/p_s at flight idle must be at least 1.03 in order to ensure reliable operation of the open fan engine. This constraint is visible in all contour plots and has to be satisfied in the engine design determination. Another limitation is the maximum propulsor rotational speed $n_{Prop,max}$, which has been set to 19.26 $\frac{1}{s}$ in consultation with DLR experts. In addition, there is an area where the multidisciplinary engine design process (see Figure 4) does not converge, meaning that the engine design is not plausible. Taking these constraints into account, an open fan design with minimal TSFC is identified

within the n_{Prop}-c_p-variation. This is localized at n_{Prop} = 18.8 $\frac{1}{s}$ and c_p = 2.2 with a $TSFC$ at Mid-CR of 15.20 $\frac{g}{kNs}$.

Apart from the TSFC, the engine mass is another important design parameter. A contour plot of the total bare open fan engine mass m_{tot} is presented in the upper right of Figure 8. m_{tot} is the sum of the total bare core engine mass $m_{tot,Core}$ and the total bare propulsor mass $m_{tot,Prop}$, whose contour plots are available in the Appendix (see Figure 12) and whose calculation is described in Section 2.4. Note that $m_{tot,Prop} = m_{Prop,Rot} + m_{Prop,Stat}$ (see Eq. (6) and Eq. (7)). In contrast to the TSFC, the sensitivity of the n_{Prop}-c_p-variation to the total bare open fan engine mass m_{tot} is considerably lower. This supports the choice of an open fan design with minimal TSFC within the conducted variation. For the selected design point, m_{tot} amounts to 3469 kg. Further details on the propulsor, performance and mass results for the determined engine design are provided in Section 3.2 and 3.2.

3.2 Propulsor Results

This section summarizes the propulsor results of the open fan design determined in Section 3.1. For this purpose, the open fan propulsor maps are evaluated, which are generated by means of the methodology described in Section 2.4 and are used in the propeller module of the performance model (see Figure 3). These maps are presented in Figure 9, together with the locations of the operating points EOF, 2ndSeg, TOC and Mid-CR (see Table 1). The propulsor data corresponding to theses operating points are listed in Table 4. Currently, MTO cannot be calculated based on the CFD-generated maps, since they contain no data at an advance ratio of zero, where MTO is located. Moreover, the flight idle operation point is plotted in Figure 9, which is defined at the advance ratio of Mid-CR and a power coefficient of zero. Note that this operation point is used in conjunction with the nozzle pressure ratio constraint considered in the n_{Prop}-c_p-variation (see Section 3.1.3).

The efficiency map is illustrated on the left side of Figure 9. Currently, an installed propulsor efficiency of 71.74 % is achieved at Mid-CR. At TOC, which is the hottest operating point in terms of the high-pressure turbine rotor inlet temperature (T41, see Table 5) and where relatively large thrust lapse effects occur, the installed propulsor efficiency is 72.17%. From an overall engine perspective, these points are important because Mid-CR is decisive for the efficiency evaluation and TOC is also a dimensioning operating point for the open fan design derived in this paper (see Table 3). Hence, it is beneficial that these points are located as close as possible to the maximum installed propulsor efficiency of the map. However, it is not possible to set the engine design point (Mid-CR, see Section 3.1.2) directly to the maximum efficiency position, because the multidisciplinary engine design process (see Figure 4) does not converge in this case. This corresponds to the area with no convergence that is marked within the n_{Prop}-c_p-variation (see Figure 8). Consequently, the determination of the open fan design is a compromise between increasing the installed propulsor efficiency and ensuring a suitable and efficient core engine design. In addition, the uninstalled propulsor efficiencies are also provided in Table 4 that are based on the propulsor gross thrust $F_{G,Prop}$ generated solely by the blading (see Figure 2 and Section 2.5). Again, the installed propulsor efficiency $\eta_{Prop,Inst}$ uses the propulsor net thrust $F_{N,Prop}$, which includes the drag of the spinner $F_{D,Spinner}$ and the nacelle $F_{D,Nacelle}$ (see Eq. (1) and Eq. (10)). The comparison between the uninstalled and installed propulsor efficiencies shows that the key operating points Mid-CR and TOC are particularly affected by the spinner and nacelle drag, since the efficiency losses amount to 7.43 % at Mid-CR and 6.44 % at TOC. To increase the installed efficiency, the reduction of the spinner and nacelle drag could be addressed in a further design iteration of the propulsor (see Section 3.5). This issue is also discussed in an accompanying paper [19] that focuses on the role of the nacelle drag in the design of open fan propulsors.

After analyzing the propulsor efficiencies, the rotor total pressure ratio $p_{t,11}/p_{t,1}$ (see Eq. (11)) and the rotor total temperature ratio $T_{t,11}/T_{t,1}$ (see Eq. (12)) are considered next. The rotor total temperature ratio is approximately 1.0 in a large region of the propulsor map (see lower right of Figure 9). Thus, no significant temperature changes occur. However, areas with pressure increases and decreases are visible in the rotor total pressure ratio map (see upper right of Figure 9).

Unfortunately, Mid-CR and TOC lie in a range with a total pressure ratio of around 0.97, which is disadvantageous on overall engine level, since the propulsor shaft power delivered by the core engine does not generate a total pressure raise in the core engine inlet (see station 11 in Figure 3) due to the flow conditions near the rotor hub section. This aspect could also be improved in a further design iteration of the propulsor (see Section 3.5). In contrast, the fan of the DLR-F25 turbofan configuration [15] achieves a total core pressure ratio of 1.22 at Mid-CR and 1.27 at TOC. At least, EOF and 2ndSeg of the open fan engine are located at total pressure ratios of approximately 1.02.

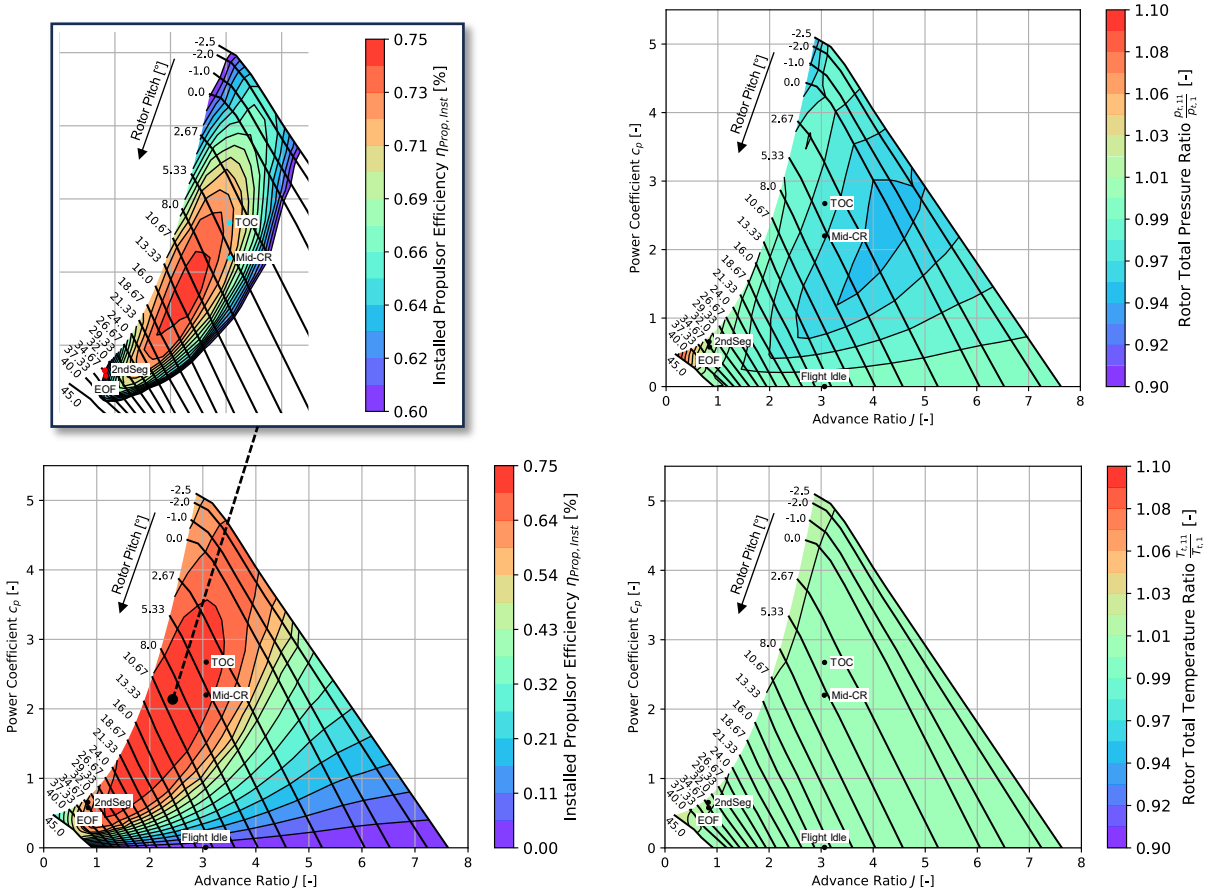


Figure 9 – Preliminary CFD-generated open fan propulsor maps for installed propulsor efficiency (left), rotor total pressure ratio (upper right) and rotor total temperature ratio (lower right) with operating point locations.

Besides the propulsor map data, Table 4 also presents aerodynamic design parameters of the combined propulsor design introduced in Section 2.4 as well as the area of the core engine inlet used in the net thrust calculation of the open fan engine (see Section 2.2). The rotor has a diameter of four meters, twelve blades, and runs at two rotational speed levels with a ratio of 1.25. The stator has ten blades and currently matches the rotor diameter. Additionally, the activity factor and sweep angle of the rotor and stator blades are provided, as they are crucial for the mass estimation of the propulsor (see Eq. (6) and Eq. (7)). Moreover, the Reynolds efficiency delta is specified in Table 4, which ranges from 1.00 % to 1.05 %. The relevance of the Reynolds number correction of the propulsor efficiency predictions is discussed in Section 2.6.2.

Table 4 – Preliminary propulsor results of the DLR open fan engine.

Parameter	Unit	EOF (Off-Design)	2ndSeg (Off-Design)	TOC (Off-Design)	Mid-CR (Design)
Rotor Diameter	[m]		4		
Rotor Blades	[-]		12		
Rotor Activity Factor	[-]		228		
Rotor Sweep Angle	[°]		40		
Stator Diameter	[m]		4		
Stator Blades	[-]		10		
Stator Activity Factor	[-]		143		
Rotor Sweep Angle	[°]		20		
Core Inlet Area	[m^2]		0.203		
Rotational Speed	[1/s]	23.50	23.50	18.80	18.80
Advance Ratio	[-]	0.84	0.83	3.07	3.06
Power Coefficient	[-]	0.58	0.66	2.67	2.20
Installed Propulsor Efficiency[a)]	[%]	62.42	60.72	72.17	71.74
Uninstalled Propulsor Efficiency[a)]	[%]	61.83	60.24	78.61	79.17
Rotor Total Pressure Ratio	[-]	1.019	1.022	0.972	0.967
Rotor Total Temperature Ratio	[-]	1.012	1.014	1.007	1.007
Rotor Pitch – Design Rotor Pitch	[°]	29.19	28.45	-1.37	0
Reynolds Efficiency Delta	[%]	1.00	1.00	1.05	1.05

a) Reynolds efficiency delta is already included in the installed and uninstalled propulsor efficiency.

3.3 Performance and Mass Results

This section presents the performance and mass results of the open fan design determined in Section 3.1. First, the performance results are considered, which are summarized in Table 5 for the operating points EOF, 2ndSeg, TOC and Mid-CR. Again, MTO cannot be calculated based on the CFD-generated maps, since they contain no data at an advance ratio of zero, where MTO is located (see Figure 9). With regard to the thermodynamic cycle temperatures, Table 5 contains the HPC outlet temperature (T3), the HPT inlet temperature (T4) and the HPT rotor inlet temperature (T41) for the evaluated operating points. According to the preliminary NOx condition discussed in Section 3.1.2, the T3 is set to 769 K at Mid-CR. The T41 limit of the MCL rating introduced in Table 2 is reached at TOC. Hence, TOC is currently the hottest operating point. Furthermore, the overall pressure ratio (OPR) is specified in Table 5 for the entire open fan engine as well as for the core engine only. Due to the total pressure ratio between the core engine inlet and the freestream condition before the open fan rotor, which is discussed as part of the propulsor results (see Figure 9), there is a discrepancy between these OPRs. For the sake of completeness, the core engine inlet mass flow and the combustor fuel to air ratio (FAR) are also provided in Table 5. Finally, preliminary values for the installed thrust-specific fuel consumption (TSFC) defined in Eq. (13) are listed in Table 5. Note that these can only be compared to those of a turbofan engine if the spinner and nacelle drag is considered in the TSFC calculation of the turbofan engine. Currently, an installed TSFC of 15.20 $\frac{\mathrm{g}}{\mathrm{kNs}}$ is achieved at Mid-CR (see also Figure 8).

Table 5 – Preliminary performance results of the DLR open fan engine.

Parameter	Unit	EOF (Off-Design)	2ndSeg (Off-Design)	TOC (Off-Design)	Mid-CR (Design)
T3	[K]	961	963	829	769
T4	[K]	1710	1739	1832	1625
T41	[K]	1627	1654	1725	1532
OPR Core Engine a)	[-]	31.8	33.1	39.6	38.2
OPR Open Fan b)	[-]	32.4	33.8	38.5	37.0
Core Engine Inlet Mass Flow	[kg/s]	37.14	37.92	14.66	13.93
FAR	[-]	0.0227	0.0237	0.0308	0.0253
Installed TSFC c)	[g/kNs]	8.62	8.33	15.12	15.20

a) OPR of the core engine is defined as $p_{t,3}/p_{t,11}$ (see Figure 3).

b) OPR of the open fan engine is defined as $p_{t,3}/p_{t,1}$ (see Figure 3).

c) The installed TSFC is defined in Eq. (13). It Includes the drag of the spinner $F_{D,Spinner}$ and the nacelle $F_{D,Nacelle}$ in the calculation of the net thrust F_N (see Eq. (1) and Eq. (4)). Hence, the installed TSFC is not comparable to a TSFC value of a turbofan engine that does not includes the spinner and nacelle drag.

After evaluating the performance results, the geometry model and mass results are considered next. Figure 10 illustrates the 2D open fan core engine geometry model of the open fan design determined in Section 3.1, including overall dimensions. The core engine geometry model is generated by means of the geometry process introduced as part of Section 2.4. As a preliminary assumption, the turbomachinery stage numbers of the DLR-F25 turbofan configuration [15] are adopted in the geometry model. Therefore, the open fan core engine consists of a three-stage booster, an eight-stage HPC, a two-stage HPT and a four-stage, fast-spinning LPT. Additionally, the basic dimensions of the core engine are shown in Figure 10. The corresponding mass results are presented in Table 6. These are estimated by using the methodology described in Section 2.4. In total, the bare core engine mass amounts to 2177 kg (gearbox mass included). The predicted bare propulsor mass is 1292 kg. This results in a bare mass estimation of 3469 kg for the entire open fan engine (see also Figure 8). Note that the nacelle mass is generally calculated by the overall aircraft design. Thrust reversers are likely not needed, since the variable pitch control of the open fan propulsor is expected to handle this function.

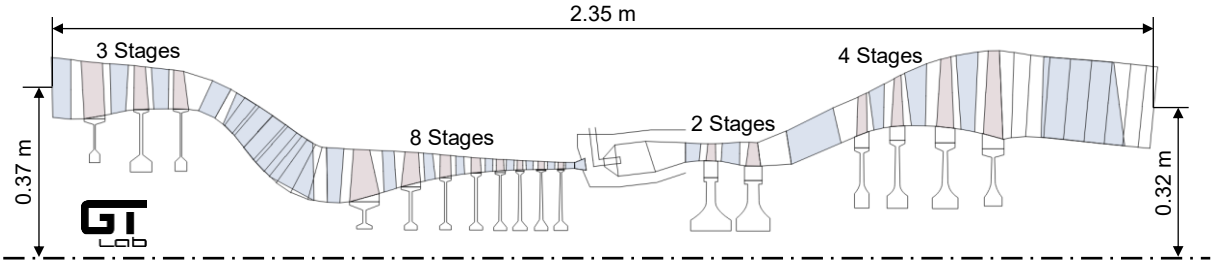


Figure 10 – Preliminary 2D open fan core engine geometry model of the DLR open fan engine.

Table 6 – Preliminary mass results of the DLR open fan engine.

Assembly	Component	Mass [kg]
Core Engine	Gearbox	412
	Booster	116
	HPC	240
	Combustor	77
	HPT	161
	LPT	394
	HP Shaft	67
	LP Shaft	94
	Frames & Ducts	163
	Accessories	453
	Bare Core Engine	2177
Propulsor	Rotor Assembly [a)]	953
	Stator Assembly [a)]	339
	Bare Propulsor	1292
Open Fan	Bare Open Fan Engine	3469

a) Includes variable pitch control and all sub-components.

3.4 Sensitivity of Aircraft Installation Effects

This paper considers an isolated open fan engine and assesses its performance and mass in the early phase of conceptual design. When the open fan engine is mounted on the aircraft wing, aerodynamic installation effects occur that can significantly affect the airflow around the propulsor and the nacelle. Consequently, important performance parameters, such as the propulsor efficiency, can also change due to these installation effects. A detailed investigation of the open fan engine installation effects under takeoff conditions is provided in [27].

Since the performance and mass results presented in Section 3.2 are calculated for an isolated open fan engine, the sensitivity of these to aircraft installation effects is estimated in this paper by varying the installed propulsor efficiency at Mid-CR. Therefore, the entire installed propulsor efficiency map is scaled in order to match the targeted installed efficiency at Mid-CR, which is also the selected engine design point (see Section 3.1.2). Figure 11 presents the sensitivity of the installed propulsor efficiency $\eta_{Prop,Inst}$ (see Eq. (10) and Table 4) to the installed thrust-specific fuel consumption $TSFC$ at Mid-CR (see Eq. (13) and Table 5) and the total bare open fan engine mass m_{tot} (see Section 3.1.3 and Table 6). A 1.0 Δ% decrease in $\eta_{Prop,Inst}$ results in an increase of $TSFC$ by 1.02 % and m_{tot} by 0.75 %. Hence, it is essential to minimize the installation effects as much as possible and to consider them in the overall design of the open fan engine and the corresponding aircraft. According to the results generated in an accompanying paper [27], the influence of installation effects on the installed propulsor efficiency at Mid-CR can be compensated by mounting the open fan engine on the aircraft wing in an appropriate manner. Details on the position of the engine in relation to the wing are provided in [27].

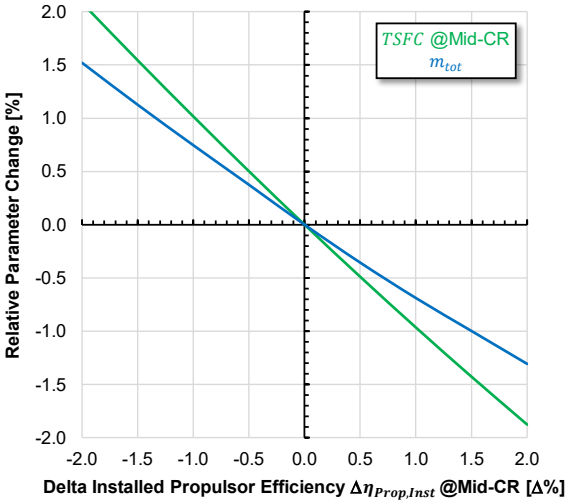


Figure 11 – Sensitivity of the installed propulsor efficiency at Mid-CR to the installed thrust-specific fuel consumption at Mid-CR and the total bare open fan engine mass.

3.5 Future Propulsor Design Goals

As part of the presentation of the propulsor results, two issues for a further design iteration of the open fan propulsor are identified (see Section 3.2). These include an increase in installed propulsor efficiency enabled by a reduction of the spinner and nacelle drag as well as the avoidance of pressure losses between the freestream conditions and the core engine inlet. In the context of aircraft installation effects (see Section 3.4), the relevance of the installed propulsor efficiency has already been demonstrated in a sensitivity analysis (see Figure 11).

Building on these issues, future design goals for the propulsor of the open fan engine are defined in Table 7. First, a 1.5 Δ% increase in installed propulsor efficiency $\eta_{Prop,Inst}$ (see Eq. (10)) at Mid-CR is envisaged. For this purpose, the entire installed propulsor efficiency map is scaled in order to match the desired installed efficiency at Mid-CR, which is also the selected engine design point (see Section 3.1.2). Second, the rotor total pressure ratio $p_{t,11}/p_{t,1}$ (see Eq. (11)) should be 1.0 at Mid-CR and TOC, where this parameter is currently around 0.97 (see Table 4). Table 7 quantifies the impact of these future propulsor design goals on the installed thrust-specific fuel consumption $TSFC$ at Mid-CR (see Eq. (13) and Table 5) and the total bare open fan engine mass m_{tot} (see Section 3.1.3 and Table 6). In accordance with Figure 11, a 1.5 Δ% increase in $\eta_{Prop,Inst}$ leads to a reduction of $TSFC$ by 1.43 % and m_{tot} by 1.00 %. When $p_{t,11}/p_{t,1}$ is set to 1.0 at Mid-CR and TOC, a decrease of $TSFC$ by 0.27 % and m_{tot} by 1.44 % is obtained. Obviously, $\eta_{Prop,Inst}$ is more sensitive to $TSFC$, whereas $p_{t,11}/p_{t,1}$ has a greater effect on m_{tot}. The latter is due to the influence of $p_{t,11}/p_{t,1}$ on the core engine inlet pressure and thus the core engine inlet mass flow. If $p_{t,11}/p_{t,1}$ is increased at the design point (Mid-CR), the core size decreases, which results in a lighter core engine. Finally, a combined setting is evaluated separately in Table 7 that considers both propulsor design goals simultaneously. In this case, a 1.73 % reduction in $TSFC$ and a 2.40 % decrease in m_{tot} are achieved.

Table 7 – Future design goals for the propulsor of the open fan engine.

Goal	Change in $TSFC$ @Mid-CR [%]	Change in m_{tot} [%]
$\eta_{Prop,Inst}$ +1.5 Δ% @Mid-CR	-1.43	-1.00
$p_{t,11}/p_{t,1}$ = 1.0 @Mid-CR and TOC	-0.27	-1.44
Combined [a)]	-1.73	-2.40

a) Calculated separately, not merely the sum of the other goals.

4. Conclusion

This paper assesses the performance and mass of an open fan engine for a short-medium range aircraft in the early phase of conceptual design. Therefore, a multidisciplinary design process is used that incorporates CFD-generated maps to model the operating behavior of the propulsor. The design process is based on an open fan performance model and a 2D core engine geometry model, which are created as part of this paper. For the estimation of the core engine and propulsor masses, a correlation-based methodology is applied. During the open fan design determination, several core engine technology limitations and a suitable design scheme are introduced. In order to identify an open fan design with minimum thrust-specific fuel consumption (TSFC), the design propulsor rotational speed and power coefficient are varied. Subsequently, the preliminary propulsor, performance and mass results are evaluated for the determined open fan design. An installed TSFC of 15.20 $\frac{\mathrm{g}}{\mathrm{kNs}}$ at Mid-CR and a total bare open fan engine mass of 3469 kg are currently achieved. Finally, the sensitivity of the performance and mass results to aircraft installation effects is investigated, followed by the definition of future propulsor design goals.

5. Outlook

This paper makes a substantial contribution to the understanding of open fan engines and presents an initial open fan design with preliminary performance and mass results. Although considerable progress has been made throughout this work, there are still various tasks that the authors intend to address in the future. The main tasks are as follows:

- Realization of the targeted propulsor design goals (see Section 3.5). This includes a 1.5 % increase in installed propulsor efficiency at Mid-CR and the avoidance of pressure losses between the freestream conditions and the core engine inlet (see Table 7).
- Calculation of operating points at low advance ratios or power coefficients within the propulsor maps, such as MTO or idle conditions (see Figure 9), using a combination of CFD-generated data and preliminary design methods. Currently, the region of small power coefficients is only covered by a simple extrapolation (see Section 2.6.1).
- Integration of emissions models in the open fan design process (see Section 2.3) and consideration of these within the design determination (see Section 3.1).
- Extension of the sketching process of the 2D geometry models to enable the generation of not only the core engine, but also the propulsor and the gearbox (see Section 2.4 and Figure 10). Subsequently, the empirical mass estimation of the propulsor and the gearbox should be replaced by a geometry-based approach (see Section 2.4).
- Due to the constant propulsor rotational speed settings (see Table 4), the low-pressure turbomachinery components currently show stability issues at EOF and 2ndSeg as well as under idle conditions. This particularly concerns the booster with regard to the surge margin. This problem should be addressed by introducing a handling bleed after the booster. Alternatively, electrical components could be used to transfer power from the low-pressure shaft to the high-pressure shaft at these operating points. A non-electrical solution might be a three-shaft architecture with an additional intermediate-pressure turbine that is connected to the booster in place of the low-pressure turbine.
- Direct comparison between the DLR-F25 turbofan configuration [15] and DLR-F25 open fan configuration. This encompasses all designs stages, ranging from the propulsor over the engine up to the aircraft.

6. Acknowledgments

The Short-Medium Range Aircraft Architecture and Technology Integration Project (SMR ACAP, project number: 101101955) is supported by the Clean Aviation Joint Undertaking and its members. **Disclaimer**: Co-Funded by the European Union. Views and opinions expressed are however those of the author(s) only and do not necessarily reflect those of the European Union or Clean Aviation Joint Undertaking. Neither the European Union nor the granting authority can be held responsible for them.



7. Contact Author Email Address

Patrick Wehrel
German Aerospace Center (DLR)
Institute of Propulsion Technology
Cologne, Germany
mailto: patrick.wehrel@dlr.de

8. Copyright Statement

The authors confirm that they, and/or their company or organization, hold copyright on all of the original material included in this paper. The authors also confirm that they have obtained permission, from the copyright holder of any third party material included in this paper, to publish it as part of their paper. The authors confirm that they give permission, or have obtained permission from the copyright holder of this paper, for the publication and distribution of this paper as part of the ICAS proceedings or as individual off-prints from the proceedings.

References

[1] European Commission *Flightpath 2050 - Europe's Vision for Aviation - Report of the High-Level Group on Aviation Research*, Brussels (Belgium), 2011, https://op.europa.eu/en/publication-detail/-/publication/296a9bd7-fef9-4ae8-82c4-a21ff48be673.

[2] European Commission *Fly the Green - Deal Europe's Vision for Sustainable Aviation - Report of the Advisory Council for Aviation Research and Innovation in Europe (ACARE)*, Brussels (Belgium), 2022, https://op.europa.eu/en/publication-detail/-/publication/69dfdaf4-07d5-11ed-acce-01aa75ed71a1.

[3] Rovira Sala, C. et al. Goals and Strategies for Open Fan Design. *International Journal of Turbomachinery, Propulsion and Power*, Vol. 10, No. 3, 2025, https://doi.org/10.3390/ijtpp10030028.

[4] Schnell, R. and Mennicken, M. Unified Assessment of Open and Ducted Propulsors. *Aerospace*, Vol. 11, No. 12, 2024, https://doi.org/10.3390/aerospace11121002.

[5] GE Aircraft Engines *Full Scale Technology Demonstration of a Modern Counterrotating Unducted Fan Engine Concept - Engine test*. NASA Contractor Report, NASA-CR-180869, 1987, https://ntrs.nasa.gov/citations/19900000733.

[6] Chapman, D. C., Godston, J. and Smith, D. E. Testing of the 578-DX Propfan Propulsion System. *AIAA/ASME/SAE/ASEE 24th Joint Propulsion Conference*, Boston (Massachusetts), 1988, https://doi.org/10.2514/6.1988-2804.

[7] GE *FAA CLEEN Program Open Rotor Engine Aeroacoustic Technology*. Final Report, 2013, https://www.faa.gov/sites/faa.gov/files/about/office_org/headquarters_offices/apl/Open_Rotor_Public_Final_Report.pdf.

[8] Suder, K. L. Overview of the NASA Environmentally Responsible Aviation Project's Propulsion Technology Portfolio. *48th AIAA/ASME/SAE/ASEE Joint Propulsion Conference & Exhibit*, Atlanta (Georgia), 2012, https://doi.org/10.2514/6.2012-4038.

[9] Hendricks, E. S. and Tong, M. T. Performance and Weight Estimates for an Advanced Open Rotor Engine. *48th AIAA/ASME/SAE/ASEE Joint Propulsion Conference & Exhibit*, Atlanta (Georgia), 2012, https://doi.org/10.2514/6.2012-3911.

[10] Schnell, R., Yin, J., Voss, C. and Nicke, E. Assessment and Optimization of the Aerodynamic and Acoustic Characteristics of a Counter Rotating Open Rotor. *Journal of Turbomachinery*, Vol. 134, No. 6, 2012, https://doi.org/10.1115/1.4006285.

[11] Diette, C. Open Fan Engine Architecture for Next Generation SMR. *33rd Congress of the International Council of the Aeronautical Sciences*, Stockholm (Sweden), 2022, https://www.icas.org/icas_archive/ICAS2022/data/papers/ICAS2022_0925_paper.pdf

[12] CFM International *RISE program: Revolutionary Innovation for Sustainable Engines*. https://www.cfmaeroengines.com/rise.

[13] Tantot, N. et al. A Performance Model for the Open Fan Propulsor. *Aerospace Europe Conference 2023 – 10th EUCASS – 9th CEAS*, Lausanne (Swiss), 2023, DOI: 10.13009/EUCASS2023-441.

[14] Chapman, J. W., Bennett, M. and Tong, M. Performance and Weight Estimates of an Open Rotor Propulsion System Concept for Next Generation Aircraft. *AIAA SciTech 2025 Forum*, Orlando (Florida), 2025, https://doi.org/10.2514/6.2025-0092.

[15] Wöhler, S., Häßy, J. and Kriewall, V. Establishing the DLR-F25 as a Research Baseline Aircraft for the Short-Medium Range Market in 2035. *34th Congress of the International Council of the Aeronautical Sciences*, Florence (Italy), 2024, https://www.icas.org/icas_archive/icas2024/data/papers/icas2024_0398_paper.pdf.

[16] Reitenbach, S. et al. Collaborative Aircraft Engine Preliminary Design using a Virtual Engine Platform, Part A: Architecture and Methodology. *AIAA SciTech 2020 Forum*, Orlando (Florida), 2020, https://doi.org/10.2514/6.2020-0124.

[17] Institute of Propulsion Technology, German Aerospace Center (DLR) *GTlab - Gas Turbine Laboratory*. https://www.gtlab.de/.

[18] Institute of Propulsion Technology, German Aerospace Center (DLR) *TRACE User Guide*. https://www.trace-portal.de/userguide/trace/index.html.

[19] Schnell, R. et al. The Role of Nacelle Drag in Open Fan Design. *27th Conference of the International Society for Air Breathing Engines*, Mumbai (India), 2026, ISABE_2026_091.

[20] Kurzke, J. and Halliwell, I. *Propulsion and Power - An Exploration of Gas Turbine Performance Modeling*. 1. Edition, Springer International Publishing AG, 2025, https://doi.org/10.1007/978-3-031-65026-0.

[21] Farokhi, S. *Aircraft Propulsion*. 2. Edition, John Wiley & Sons Ltd, 2014, https://www.wiley-vch.de/en/areas-interest/engineering/mechanical-engineering-10me/aeronautic-aerospace-engineering-10me7/aircraft-propulsion-978-1-394-26311-0.

[22] Häßy, J., Bolemant, M. and Becker, R. G. An Educated Guess - Predicting Turbomachinery Efficiencies of Aero Engines During Conceptual Design. *ASME Turbo Expo 2024: Power for Land, Sea, and Air*, Boston (Massachusetts), 2023, https://doi.org/10.1115/GT2023-103638.

[23] Häßy, J. and Schmeink, J. Knowledge-Based Conceptual Design Methods for Geometry and Mass Estimation of Rubber Aero Engines. *33rd Congress of the International Council of the Aeronautical Sciences*, Stockholm (Sweden), 2022, https://www.icas.org/icas_archive/ICAS2022/data/papers/ICAS2022_0497_paper.pdf.

[24] Wehrel, P., Schmeink, J and Häßy, J. Knowledge-Based Turbine Disk Modeling - A Conceptual Design Process Calibrated to the NASA Energy Efficient Engine. *34th Congress of the International Council of the Aeronautical Sciences*, Florence (Italy), 2024, https://www.icas.org/icas_archive/icas2024/data/papers/icas2024_0272_paper.pdf.

[25] Klees, G. W. and Fishbach, L. H. Aircraft Engine Weight Estimation Method. *37th Annual Conference of the Society of Allied Weight Engineers, Inc.*, Munich (Germany), 1978, https://www.sawe.org/product/paper-1248/.

[26] Strack, W. C. et al. *Technology and Benefits of Aircraft Counter Rotation Propellers*. NASA Technical Memorandum, NASA-TM-82983, 1982, https://ntrs.nasa.gov/citations/19830002859.

[27] Stürmer, A. W. Engine-Airframe Installation Effects for Open Fan Powered Aircraft at Take-Off Conditions. *AIAA Aviation Forum and ASCEND 2024*, Las Vegas (Nevada), 2024, https://arc.aiaa.org/doi/10.2514/6.2024-3518.

Appendix

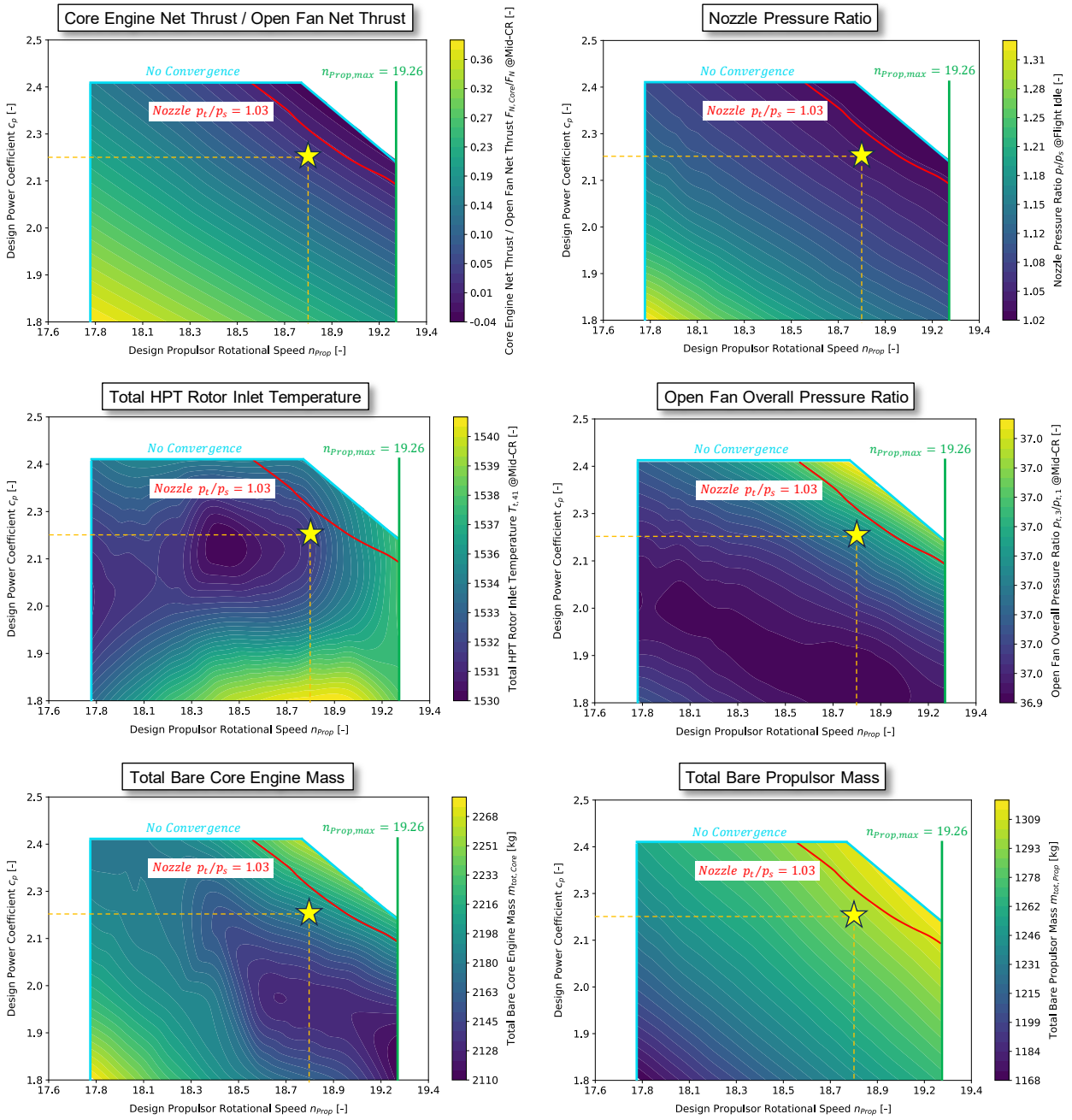


Figure 12 – Contour plots for several performance and mass parameters generated in the variation of the design propulsor rotational speed and power coefficient.